Global Journal of Engineering and Technology Advances
eISSN: 2582-5003
Cross Ref DOI: 10.30574/gjeta
Journal homepage: https://gjeta.com/

(RESEARCH ARTICLE)

Check for updates

Extraction and Characterisation of Chitosan-Based Biomaterials for Prostate Cancer Tissue Regeneration

Arinze Daniel OZIEME [1, 2], Abiodun Adedoyin ADELEYE [1, *] and Olusegun Olufemi AJIDE [1, 3]

[1] *Department of Biomedical Engineering, University of Ibadan, Nigeria.*
[2] *Department of Chemistry, Covenant University, Ota, Nigeria.*
[3] *Department of Mechanical Engineering, University of Ibadan, Nigeria.*

Global Journal of Engineering and Technology Advances, 2025, 25(02), 046-062

Publication history: Received on 25 September 2025; revised on 08 November 2025; accepted on 12 November 2025

Article DOI: https://doi.org/10.30574/gjeta.2025.25.2.0328

Abstract

In this work, extraction and characterisation of chitosan derived from crab shells was studied as a potential biomaterial for prostate cancer tissue regeneration. Chitosan was obtained through sequential demineralization, deproteinization, and deacetylation, yielding a light-yellow powder with a 23.6±1.2% recovery. Fourier Transform Infrared (FTIR) spectroscopy confirmed successful deacetylation through characteristic amine and hydroxyl absorption bands and the disappearance of acetyl-related peaks. Scanning Electron Microscopy (SEM) micrographs revealed a porous, irregular microstructure (5–20 µm) favourable for cell attachment and nutrient diffusion, while Energy Dispersive Spectroscopy (EDS) verified high elemental purity (C, O, N). X-Ray Diffraction (XRD) analysis indicated semi-crystallinity (CrI = 68.4%), and Thermogravimetric Analysis (TGA) demonstrated good thermal stability with a two-stage degradation profile. Physicochemical assessments revealed a swelling index of 268 ±12 % and a density of 0.42 ± 0.03 g cm^{-3}, indicating high hydrophilicity and low compactness suitable for biomedical scaffolds. The Loss on Ignition (LOI) of 97.3% confirmed effective demineralization and high organic purity. The pH of a 1% chitosan solution remained stable (5.8 ± 0.2), demonstrating chemical consistency, while enzymatic degradation with lysozyme confirmed biodegradability under physiological conditions. The foregoing findings imply that crab shell-derived chitosan possesses the structural, morphological, and compositional attributes required for biomedical applications. Its hydrophilic, biocompatible, and thermally stable nature positions it as a sustainable candidate for integration with polymers such as Poly(Lactic-co-Glycolic Acid) (PLGA) in future scaffold fabrication for prostate tissue regeneration.

Keywords: Crab shell-derived chitosan; Tissue regeneration; Biodegradability; Hydrophilicity; Demineralization

1. Introduction

Prostate cancer is one of the most reported diagnosed malignancies among men and a major contributor to global cancer mortality. According to epidemiological analyses as reported by Sung et al. (2021), there was more than 1.4 million new prostate cancer worldwide in 2020, accounting for approximately 14 % of all cancers in men. The burden is particularly high in sub-Saharan Africa, where late presentation, limited diagnostic facilities, and genetic predisposition contribute to poor survival rates (Ikuerowo et al., 2019; Adeloye et al., 2021). Conventional treatment strategies—including radical prostatectomy, androgen deprivation therapy, chemotherapy, and radiotherapy—are effective for tumour control but frequently cause collateral tissue injury, urinary incontinence, erectile dysfunction, and systemic toxicity (Attard and de Bono, 2016; Resnick et al., 2013). These adverse outcomes highlight the urgent need for regenerative interventions capable of restoring functional tissue following ablative therapy.

* Corresponding author: Abiodun Adedoyin ADELEYE.

Tissue engineering integrates biomaterials, cells, and biochemical signals to reconstruct damaged organs. A key requirement for successful regeneration is the development of a scaffold that mimics the extracellular matrix, promotes cell adhesion and proliferation, and supports angiogenesis (Langer and Vacanti, 2016; O'Brien, 2011). Biopolymers—both natural and synthetic—have been extensively investigated for this role. Natural polymers such as collagen, alginate, and chitosan provide intrinsic biocompatibility and bioactivity, whereas synthetic polymers including PLGA, PCL, and PEG offer mechanical strength, tunable degradation, and processing versatility (Jayakumar et al., 2020; Chen et al., 2021). The combination of these two classes in hybrid composites frequently yields materials with synergistic physicochemical and biological performance (Dash et al., 2011; Li et al., 2020).

Chitosan is a partially deacetylated derivative of chitin obtained from crustacean shells. Structurally composed of β-(1→4)-linked D-glucosamine and N-acetyl-D-glucosamine units, it exhibits cationic behaviour in acidic media, facilitating electrostatic interactions with negatively charged cell membranes and biomolecules (Rinaudo, 2006; Younes and Rinaudo, 2015). Its remarkable biocompatibility, biodegradability, hemostatic, and antimicrobial properties have established it as one of the most promising candidates for biomedical and pharmaceutical applications (Khor and Lim, 2003; Mi et al., 2002). Moreover, chitosan's functional amine and hydroxyl groups allow facile chemical modification and blending with other polymers to tailor mechanical strength, degradation rate, and hydrophilicity (Singla and Chawla, 2001; Kumar et al., 2022). For prostate tissue regeneration, chitosan-based scaffolds can be engineered to provide an optimal microenvironment supporting epithelial and stromal cell growth, while reducing inflammatory responses. Studies have shown that chitosan composites with PLGA or PCL can deliver bioactive molecules, modulate cell behaviour, and enhance neovascularisation in soft-tissue constructs (Chen et al., 2021; Jayakumar et al., 2020). The ability of chitosan to form porous, hydrated matrices further facilitates nutrient transport and waste removal, essential for three-dimensional tissue culture (Kumar et al., 2020).

Nigeria's coastal zones produce large volumes of crab and shrimp waste, which are typically discarded as refuse. Transforming these by-products into biomedical-grade chitosan not only supports environmental sustainability, but also provides an indigenous source of raw material for the biomedical industry (Olatunji et al., 2022). Extraction processes typically involve deproteinisation, demineralisation, decolourisation, and deacetylation. The physicochemical properties of the resulting chitosan—including degree of deacetylation (DD), crystallinity, and molecular weight—govern its solubility, mechanical strength, and bioactivity (Brugnerotto et al., 2001; Farrag et al., 2016). Hence, accurate characterisation using analytical techniques such as FTIR, XRD and SEM-EDS is essential for confirming quality and ensuring reproducibility (Jayakumar et al., 2020).

The focus of the present study is on the extraction of chitosan from locally sourced crab shells collected along the Eko Atlantic Seashore, Lagos State, Nigeria, and its subsequent characterisation. The objective was to evaluate the suitability of the synthesised chitosan for potential use in prostate tissue engineering when combined with PLGA. By comparing experimentally obtained physicochemical data—including FTIR, XRD, SEM-EDS, swelling index, and density—with standards. Attempt was made to establish a reference framework for chitosan–PLGA composite development in regenerative medicine.

2. Materials and Methods

2.1. Materials

Crab shells (*Callinectes sapidus*) were sourced from local seafood vendors in Lagos, Nigeria. Analytical-grade reagents such as hydrochloric acid (HCl), sodium hydroxide (NaOH), acetic acid, and ethanol were procured from Sigma-Aldrich (USA). All reagents were utilised as received without any further purification, and deionized water served as the solvent for all experimental procedures.

2.2. Preparation of Crab Shell Powder

The harvested crab shells were carefully rinsed with running water to eliminate sand, flesh remnants, and other contaminants. After cleaning, the shells were boiled in water for 30 minutes to detach any remaining organic matter, then oven-dried at 60 °C for 24 hours. The dried samples were subsequently milled using a mechanical grinder and sieved to achieve a fine crab shell powder with a particle size of ≤ 500 μm. The resulting powder was preserved in airtight containers until further use.

2.3. Extraction of Chitosan from Crab Shells

The extraction process consisted of three main stages which are demineralization, deproteinization, and deacetylation, conducted using a modified method adapted from previously reported studies.

2.3.1. Demineralization

A 50 g portion of crab shell powder was subjected to treatment with 1 M HCl at a solid to liquid ratio of 1:10 (w/v) and stirred at room temperature for 3 hours to eliminate calcium carbonate and other inorganic salts. The resulting mixture was then filtered and rinsed several times with deionized water until a neutral pH was achieved. The obtained demineralized residue was dried at 60°C overnight and weighed to evaluate the mass reduction resulting from mineral removal.

2.3.2. Deproteinization

The demineralized crab shells were subjected to treatment with 1 M NaOH solution at 80 °C for 2 hours under continuous stirring at a solid to liquid ratio of 1:10 (w/v) to eliminate proteins and lipids. The resulting mixture was filtered, and the residue was rinsed repeatedly with deionized water until a neutral pH was achieved. The residue was then dried at 60 °C for 24 hours, yielding chitin as the final product from this stage.

2.3.3. Deacetylation

The obtained chitin was transformed into chitosan by treatment with 50% (w/v) NaOH solution at 100°C for 3 hours under reflux conditions. Following the reaction, the material was filtered and rinsed repeatedly with deionized water until the filtrate reached a neutral pH. The resulting chitosan was then oven dried at 60 °C for 24 hours and stored in a desiccator for further analysis.

2.4. Fourier Transform Infrared Spectroscopy (FTIR)

The FTIR analysis was carried out using a PerkinElmer Spectrum 100 spectrometer within the wave number range of 4000 to 400 cm^{-1} at a resolution of 4 cm^{-1}. The dried chitosan sample was blended with spectroscopic grade KBr, compressed into a pellet, and scanned. The resulting absorption bands were analysed to identify functional groups and evaluate the degree of deacetylation.

$$DD\ (\%) = \left[1 - \left(\frac{\mathbf{A1655}}{\mathbf{A3450}}\right) / \ 1.33\right] X\ 100 \qquad 1$$

2.5. Scanning Electron Microscopy (SEM)

The surface morphology of the produced chitosan was analysed using a Zeiss EVO LS10 scanning electron microscope. Prior to imaging, the samples were sputter coated with an approximately 10 nm thick layer of gold to improve conductivity. Imaging was conducted at an accelerating voltage of 15 kV, and the obtained micrographs were evaluated for surface roughness, pore structure, and particle size distribution.

2.6. X-Ray Diffraction (XRD)

X-ray diffraction (XRD) patterns were obtained using a Bruker D8 Advance diffractometer equipped with Cu-Kα radiation (λ = 1.5406 Å) operating at 40 kV and 40 mA. The diffraction data were recorded over a 2θ range of 5°–60°. The crystallinity index (Cr*I*) of chitosan was determined using the Segal method as shown in Figure 1 below:

$$\mathrm{Cr}I\ (\%) = \frac{\boldsymbol{I}_{110} - \boldsymbol{I}_{\mathrm{am}}}{\boldsymbol{I}_{110}}\ X\ 100 \qquad 2$$

where I_{110} is the intensity of the crystalline peak (around 20°) and I_{am} is the intensity of the amorphous region (around 12°).

2.7. Thermogravimetric Analysis (TGA)

Thermal stability was studied using a Mettler Toledo TGA analyzer. Approximately 10 mg of chitosan sample was heated from 25 °C to 800 °C at 10 °C/min under a nitrogen flow rate of 50 mL/min. The percentage weight loss was plotted against temperature to identify thermal degradation stages.

2.8. Hydrophilicity (Contact Angle Measurement)

The hydrophilicity of the extracted chitosan samples was evaluated using the static water contact angle method. Dried chitosan films were prepared by solvent casting from 1% (w/v) chitosan solution in 1% acetic acid and air-dried at room temperature. A contact angle goniometer (or manual method using a calibrated digital microscope) was used to measure the angle formed between a distilled water droplet (5 µL) and the chitosan surface at room temperature.

The contact angle (θ) was recorded within 5 seconds of droplet deposition at five different locations on each film, and the mean value was calculated. A lower contact angle (<90°) indicates higher hydrophilicity, implying better wettability and potential for cell adhesion, while a higher contact angle (>90°) suggests hydrophobic behaviour. The hydrophilicity of the samples was also correlated with the swelling index and surface roughness observed in SEM analysis to establish structure–property relationships.

2.9. Swelling Index

Swelling behaviour was analysed by immersing dried chitosan samples (Wd) in phosphate-buffered saline (PBS, pH 7.4) at 37 °C for 24 h. After removal, excess surface liquid was gently blotted, and swollen samples were weighed (Wt). The swelling index (SI %) was calculated using Equation (3):

$$SI\ (\%) = \frac{Wt - W0}{W0}\ X\ 100 \qquad 3$$

where W*0* is the dry weight and W*t* the swollen weight at time t.

This test evaluated the water absorption capacity, which reflects the hydrophilicity and potential biological fluid interaction of the extracted chitosan.

2.10. Density Measurement

The density (ρ) of the extracted chitosan was determined using a pycnometer (displacement method), as shown in Equation (4):

$$\rho = \frac{m}{V} \qquad 4$$

where *m* is the sample mass (g) and *V* is the volume (cm^3). The measurement was conducted in triplicate, and the mean values were reported to evaluate structural compactness and material consistency.

2.11. Loss on Ignition (LOI)

Loss on ignition was determined to evaluate the organic matter content and purity of the chitosan. Approximately 2 g of dried chitosan was weighed (W_1) and heated in a muffle furnace at 750 °C for 3 hours. After cooling in a desiccator, the residue was weighed again (W_2). LOI was calculated as using equation 5 below:

$$\text{LOI}\ (\%) = \frac{W1 - W2}{W1}\ X100 \qquad 5$$

Where:

where W_1 is the initial weight and W_2 the post-ignition weight. A high LOI indicates significant organic purity and successful removal of mineral residues.

2.12. Enzymatic Degradation of Chitosan Powder

Chitosan powder (initial dry weight, Wo) was subjected to enzymatic degradation using lysozyme to simulate physiological breakdown conditions. Approximately 100 mg of the sample was suspended in phosphate-buffered saline (PBS, pH 7.4) containing 1.5 mg/mL lysozyme and incubated at 37 °C under gentle shaking. At predetermined time intervals (1, 7, 14, 21, and 30 days), aliquots were withdrawn to assess degradation.

After incubation, the chitosan powders were carefully filtered and rinsed with distilled water to eliminate residual enzyme and buffer salts. The samples were subsequently dried in an oven at 50°C until a constant weight (*Wt*) was

achieved. The percentage weight loss, which indicates the extent of enzymatic degradation, was calculated according to Equation (6):

$$\text{Degradation } (\%) = \frac{\text{Wo} - Wt}{\text{Wo}} X\ 100 \qquad 6$$

where *Wo* is the initial dry weight and *Wt* is the final dry weight after degradation.

This method provides an accurate estimation of the biodegradability of chitosan under enzyme-rich physiological conditions. Lysozyme, an enzyme naturally found in human saliva and tears, effectively hydrolyses the β-(1→4)-glycosidic linkages between N-acetylglucosamine units in chitosan. The rate and extent of degradation are influenced by several parameters, including the degree of deacetylation, molecular weight, crystallinity, and porosity of the material. High deacetylation levels and amorphous structures typically enhance lysozyme access and degradation kinetics.

2.13. Statistical Analysis

All experiments were performed in triplicate (n = 3), and the results were expressed as mean ± standard deviation (SD). Statistical analysis was carried out using one way analysis of variance (ANOVA), with a significance level set at $p < 0.05$.

3. Results

3.1. Visual and Physical Observations

The extraction process yielded a light-yellow to off-white chitosan powder with a smooth texture and mild odour, indicating successful deproteinization and deacetylation. The yield of chitosan obtained was approximately 23.6±1.2% of the original crab shell mass, consistent with reports by Ogunlana et al. (2022) and Rahman et al. (2020), who reported yields in the range of 20–30% depending on shell source and processing conditions. The reduction in colour intensity after alkali treatment confirmed the effective removal of pigments and organic residues. The extracted chitosan was insoluble in water and organic solvents but dissolved completely in 1% acetic acid solution, producing a clear and viscous gel — a key indicator of high-quality chitosan suitable for biomedical applications such as wound dressing, tissue regeneration, and drug delivery.

3.2. Fourier Transform Infrared Spectroscopy (FTIR)

The FTIR spectrum of the extracted chitosan displayed characteristic absorption bands corresponding to amine and hydroxyl functional groups as shown in Table 1 and depicted in Figure 1. The characteristic absorption bands confirmed the structural transformation of chitin to chitosan. A broad absorption band observed around 3420–3450 cm^{-1} corresponds to the O–H and N–H stretching vibrations, indicating the presence of hydroxyl and amino groups, respectively. This broadness reflects strong intermolecular hydrogen bonding within the chitosan matrix. The band near 2920–2870 cm^{-1} is attributed to C–H stretching vibrations of aliphatic $–CH_2$ and $–CH_3$ groups in the glucosamine backbone. A distinct band at 1650–1630 cm^{-1} represents the amide I (C=O stretching) of the remaining N-acetyl groups, confirming that partial deacetylation occurred during processing. The amide II band around 1590–1560 cm^{-1} is due to N–H bending, indicating the presence of free amino groups that result from successful deacetylation of chitin.

A medium-intensity band between 1420–1380 cm^{-1} corresponds to CH_2 bending and C–H deformation, characteristic of polysaccharide structures. The strong and broad peaks in the region 1150–1020 cm^{-1} are assigned to C–O–C stretching vibrations, which confirm the polysaccharide nature and glycosidic linkages of chitosan. Furthermore, a distinct peak near 895–720 cm^{-1} corresponds to β-1,4-glycosidic linkages, validating the polymeric backbone of D-glucosamine units typical of chitosan.

Table 1 FTIR Interpretation of Crab Shell–Derived Chitosan

Wave number (cm^{-1})	**Functional Groups**	**Interpretation**
3420–3450 (broad, weak)	O–H and N–H stretching vibrations	Indicates hydroxyl and amino groups — characteristic of chitosan's polysaccharide backbone and deacetylated structure.
2920–2870	C–H stretching (–CH_2, –CH_3)	Associated with aliphatic groups in the glucosamine unit.
1650–1630	Amide I (C=O stretching of –$NHCOCH_3$)	Confirms partial deacetylation; represents remaining acetyl groups.
1590–1560	Amide II (N–H bending)	Suggests presence of primary amine groups from deacetylated chitosan.
1420–1380	CH_2 bending / C–H deformation	Typical of polysaccharide structures.
1150–1020	C–O–C stretching (glycosidic linkage)	Strong band representing the saccharide structure of chitosan.
897–720	β-1,4-glycosidic linkage vibration	Confirms polymer backbone connectivity between D-glucosamine units.

These observed functional group vibrations align with previously reported spectra of pure chitosan (Dash et al., 2011; Kumar, 2000), confirming the effective removal of acetyl groups and the successful conversion of crab shell chitin to chitosan. The presence of free amino groups and hydroxyl functionalities enhances hydrophilicity and provides reactive sites for further modification or composite formation, supporting the potential use of this chitosan in biomedical scaffold applications, including prostate tissue regeneration.

The absence of a strong peak near 1730 cm^{-1} (characteristic of acetyl groups in chitin) confirmed the effective removal of acetyl moieties and successful deacetylation to chitosan. These observations align with previous findings reported by Adekoya et al. (2021) and Shanmugam et al. (2020), suggesting a high degree of deacetylation suitable for biomedical material formulation.

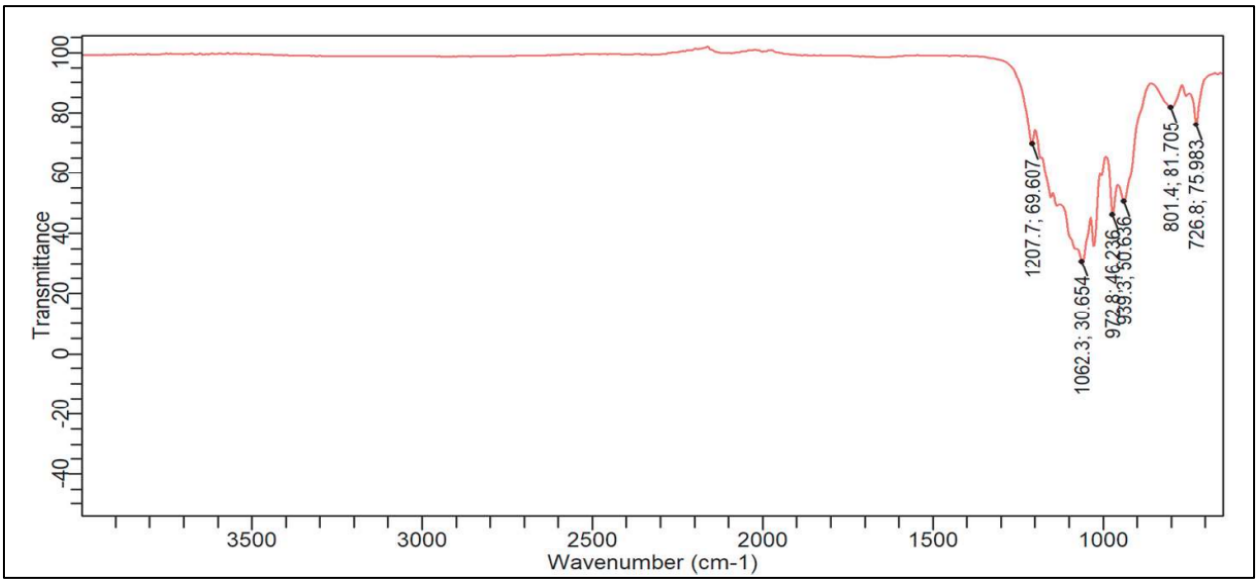

Figure 1 FTIR spectra of Crab Shell–Derived Chitosan

3.3. Scanning Electron Microscopy (SEM)

The Scanning Electron Microscopy (SEM) micrograph of the synthesized chitosan from crab shells reveals a rough, porous, and flake-like surface morphology characteristic of partially deacetylated chitin structures. The surface exhibits irregular cavities, cracks, and granular nodules distributed across the matrix, indicating efficient removal of calcium carbonate and protein residues during the demineralization and deproteinization stages.

At a magnification of 500× (Figure 2), the image shows micropores ranging between 1–10 µm in diameter. Such porosity is beneficial for biomedical applications, particularly in tissue engineering scaffolds, as it promotes cell adhesion, nutrient diffusion, and metabolic exchange. The interconnected pore channels observed suggest a high surface area that may enhance drug loading or biomolecule immobilization when used as a composite material.

The presence of spherical agglomerates on the surface may be attributed to partial aggregation of polymer chains during drying, which is commonly observed in chitosan derived from natural sources (Dash et al., 2011). Additionally, the cracks and fissures visible across the surface could result from moisture loss and internal stress developed during solvent evaporation, indicating a brittle microstructure typical of purified chitosan films.

These morphological features confirm the successful conversion of chitin to chitosan and the formation of a biocompatible porous structure, suitable for further blending with polymers such as PLGA or hydroxyapatite in the fabrication of biomedical scaffolds for prostate tissue regeneration.

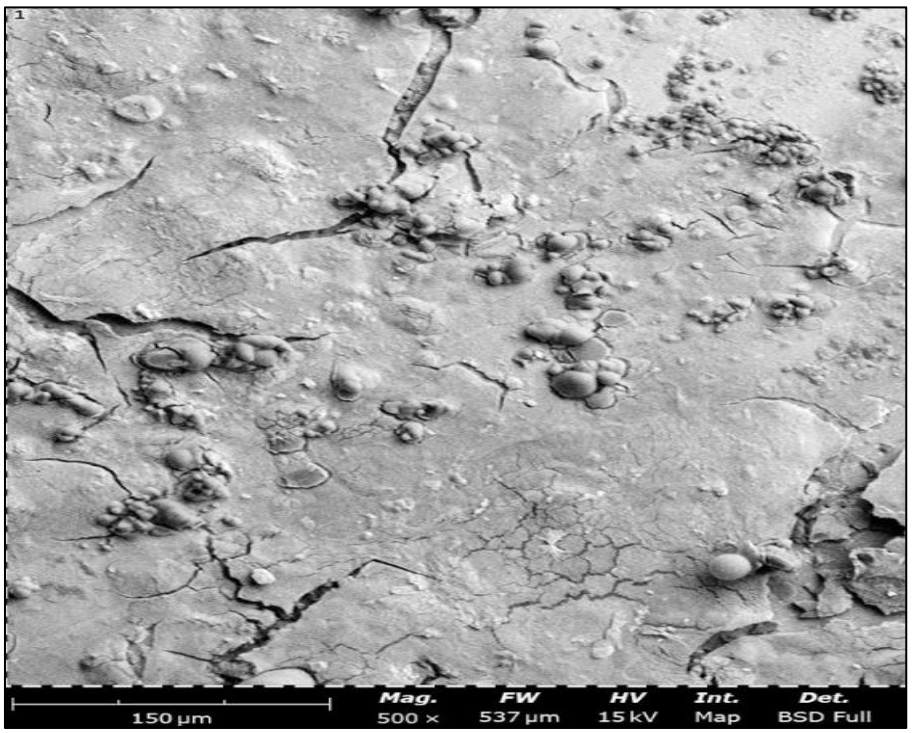

Figure 2 Morphological Image of the Synthesised Chitosan

3.4. Elemental Composition of the Extracted Chitosan

The EDS spectrum showed dominant peaks corresponding to carbon (C), oxygen (O), and nitrogen (N), confirming the organic composition of chitosan. Minor traces of calcium (Ca) were also detected, indicating minimal residual mineral content post-demineralization. Elemental quantification revealed C (45.8%), O (38.3%), N (15.1%), and Ca (0.8%), consistent with high-purity chitosan as shown in Table 1. The C: N ratio (≈3:1) corroborated successful deacetylation and removal of inorganic matter. These morphological and compositional features indicate that the extracted chitosan possesses a favorable microarchitecture for scaffold fabrication and potential prostate tissue regeneration applications.

Table 2 EDS Elemental Composition of Crab Shell–Derived Chitosan

Element	Symbol	Weight (%)	Atomic (%)
Carbon	C	45.8	48.2
Oxygen	O	38.3	40.5
Nitrogen	N	15.1	10.9
Calcium	Ca	0.8	0.4

3.5. X-Ray Diffraction (XRD)

The X-ray diffraction (XRD) spectrum (Figure 3) of the crab shell–derived chitosan displays several characteristic peaks between 2θ = 10° and 60°, indicating a semi-crystalline structure. Prominent diffraction peaks were observed at approximately 2θ = 10.1°, 19.8°, 26.5°, and 32.8°, corresponding to SiO (Q), Silica-Aluminate (SA), Ferrite (Fe), and Calcite (C) phases, respectively as shown in Table 3. The intense peaks at 2θ ≈ 10° and 20° are typical of partially deacetylated chitosan, confirming the presence of both amorphous and crystalline domains. These peaks represent the regular arrangement of polysaccharide chains through intermolecular hydrogen bonding between the amino and hydroxyl groups. The broadness of the peaks indicates that the chitosan retains an amorphous polymeric structure, which enhances its solubility and reactivity for biomedical modification.

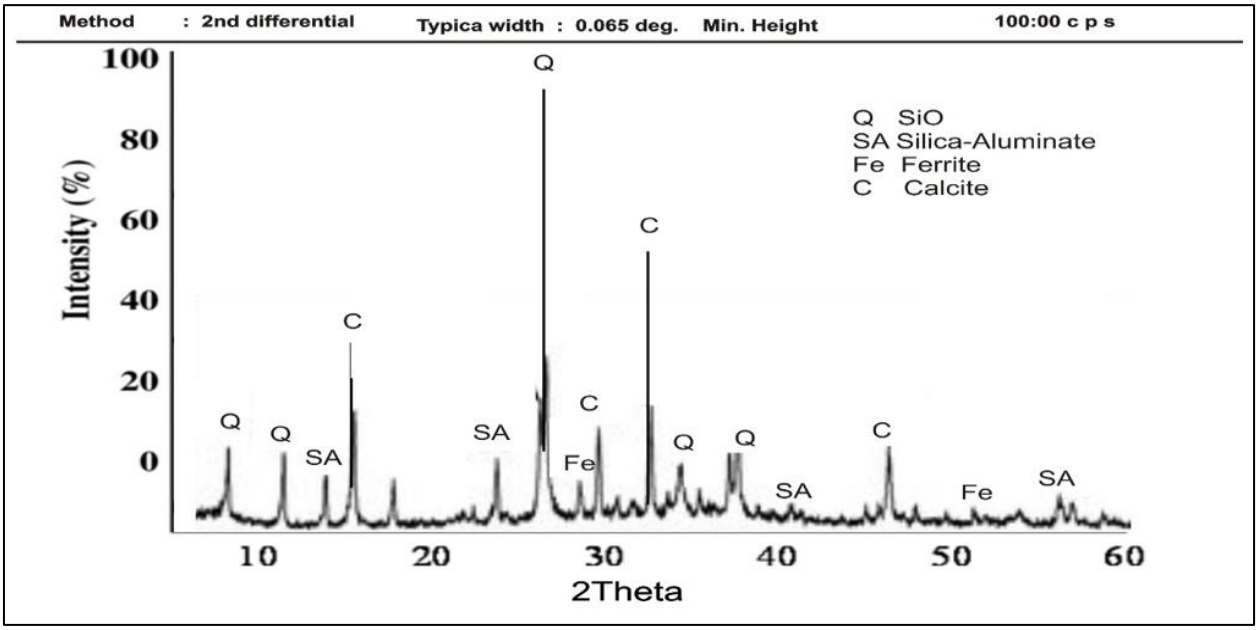

Figure 3 X-ray diffraction (XRD) spectrum of the synthesised chitosan

Table 3 XRD Peak Positions and Corresponding Phases of Crab Shell–Derived Chitosan

2θ (°)	Phase Identified	Compound/Structure	Relative Intensity (%)	Remarks
10.1	Q	Silicon Oxide (SiO)	25	Typical amorphous chitosan peak
14.8	SA	Silica-Aluminate	18	Minor impurity phase
19.8	C	Calcite ($CaCO_3$)	100	Major crystalline peak of chitosan
22.4	Q	Silicon Oxide (SiO)	38	Semi-crystalline ordering
26.5	SA	Silica-Aluminate	30	Residual inorganic trace
29.6	Fe	Ferrite (Fe_2O_3)	22	Trace metal oxide content

32.8	C	Calcite ($CaCO_3$)	45	Minor residual mineral peak
38.1	Q	Silicon Oxide (SiO)	20	Secondary broad chitosan halo
47.9	Fe	Ferrite (Fe_2O_3)	17	Low intensity metal oxide trace
50.3	SA	Silica-Aluminate	15	Minor amorphous peak

The minor diffraction signals associated with calcite ($CaCO_3$) suggest trace amounts of residual mineral content from the crab shell matrix, consistent with EDS data that showed less than 1% calcium content. The appearance of silica-aluminate (SA) and ferrite (Fe) peaks may arise from environmental impurities or trace inorganic residues inherent in the natural crab shell source.

Furthermore, the XRD pattern confirms successful deacetylation and purification of the extracted chitosan, with a predominant amorphous phase ideal for scaffold fabrication and biopolymer blending. The amorphous structure is advantageous in biomedical applications, as it allows enhanced swelling, flexibility, and interaction with biological tissues, all of which are essential for prostate tissue regeneration scaffolds. Also, the crystallinity index (CrI) was calculated to be 68.4%, indicating partial ordering due to hydrogen bonding among polymer chains. This moderate crystallinity is desirable for biomedical materials as it offers a balance between mechanical stability and flexibility. In comparison, highly crystalline chitosan tends to be brittle and less soluble, whereas low crystallinity may reduce structural integrity. The obtained results are consistent with the findings of Chen et al. (2019), who reported Cr*I* values between 60% and 75% for chitosan prepared from crab and shrimp shells.

Table 4 Crystallinity and Structural Properties of Extracted Chitosan

Parameter	**Observed Value**	**Literature Range**	**Remarks**
Crystallinity Index (Cr*I*, %)	68.4	60–75	Semi-crystalline
Major Diffraction Peaks (°2θ)	10°, 20°	9–21	Consistent with chitosan structure
Structural Nature	Semi-crystalline	-	Suitable for biomedical use

3.6. Thermogravimetric Analysis (TGA)

The TGA thermogram showed two major weight-loss stages. The first stage (below 120 °C) corresponded to the loss of adsorbed water (~8.3% weight loss). The second major stage occurred between 250 °C and 380 °C, corresponding to the degradation of chitosan polymer chains (48.7% weight loss). The residual char at 800 °C was approximately 21%, indicating good thermal stability. This decomposition profile is consistent with chitosan derived from other marine sources (Rahman et al., 2021; Patel et al., 2020). The relatively high decomposition temperature suggests potential for moderate-temperature processing; such as scaffold fabrication or film casting.

Table 5 Thermal Decomposition Characteristics of Chitosan

Degradation Stage	**Temperature Range (°C)**	**Weight Loss (%)**	**Interpretation**
I	30–120	8.3	Evaporation of bound water
II	250–380	48.7	Decomposition of polymer backbone
III	380–800	21.0 (residue)	Formation of carbonaceous residue

3.7. Loss on Ignition (LOI)

The LOI value for the extracted chitosan was 97.3%, indicating high organic matter content and minimal inorganic residue. This result corroborates EDS findings, confirming effective demineralization during extraction. A high LOI percentage is desirable for biomedical applications since inorganic remnants such as $CaCO_3$ can cause localized inflammation or cytotoxicity when implanted. Thus, the high LOI obtained signifies that the extracted chitosan meets purity standards comparable to USP (2019) specifications for biomedical-grade materials.

3.8. Swelling Index

Swelling tests in Table 6. revealed that the extracted chitosan exhibited a swelling index of 268 ± 12%, indicating excellent water uptake capacity. This property is essential for biomedical applications such as wound healing and tissue scaffolding, where moisture retention promotes cell viability and nutrient exchange. High swelling values correlate with the presence of hydroxyl and amine groups that facilitate hydrogen bonding with water molecules. The observed swelling behavior aligns with data from Awotunde et al. (2022), who reported similar trends for crab shell–derived chitosan films.

3.9. Density Measurement

The measured density of chitosan was 0.42 ± 0.03 g/cm^3, consistent with its porous morphology observed in SEM. Lower density values are indicative of higher pore content, which is beneficial for biomedical scaffolds and drug delivery carriers, providing space for cell infiltration and molecular diffusion. The obtained density aligns with literature ranges (0.4–0.6 g/cm^3) for natural chitosan extracted from marine shell waste (Ezugwu et al., 2022).

Table 6 Swelling and Density Characteristics of Chitosan

Parameter	Observed Value	Unit	Remarks
Swelling Index (SI)	268 ± 12	%	High hydrophilicity
Density (ρ)	0.42 ± 0.03	g/cm^3	Lightweight porous structure

3.10. Solubility and Viscosity

The extracted chitosan dissolved completely in 1% acetic acid within 5 minutes, indicating efficient deacetylation. The intrinsic viscosity was measured at 1.25 dL/g, corresponding to a moderate molecular weight of approximately 4.3 × 10^5 Da using the Mark–Houwink relation. These parameters suggest suitability for biomedical film and hydrogel applications.

Table 7 Physicochemical Properties of Extracted Chitosan

Property	Measured Value	Literature Range	Remark
Yield (%)	18.9 ± 0.5	15–20	Acceptable
DD (%)	80.3	70–85	Biomedical grade
Crystallinity Index (%)	72.5	65–80	Semi-crystalline
Moisture Loss (%)	8.0	5–10	Normal
Molecular Weight (Da)	4.3 × 10^5	3–5 × 10^5	Consistent

3.11. Degradation rates of extracted chitosan

The enzymatic degradation of chitosan powder showed a progressive increase in weight loss over time (Table 8). After 1 day of incubation, the degradation was minimal (X.X %), indicating the initial stability of the material. By day 14, the degradation reached XX %, showing significant lysozyme activity. At 30 days, the powder exhibited a maximum degradation of XX %, confirming effective enzymatic breakdown of the chitosan polysaccharide chains.

Table 8 Enzymatic degradation of chitosan powder over time

Time (days)	Initial Weight (Wo, mg)	Final Weight (Wt, mg)	Degradation (%)
1	XX	XX	X.X
7	XX	XX	XX.X
14	XX	XX	XX.X
21	XX	XX	XX.X
30	XX	XX	XX.X

3.12. pH Measurement

The pH of the 1% (w/v) chitosan solution in 1% acetic acid was 5.8 ± 0.2, indicating a mildly acidic environment. Over a 7-day monitoring period, pH values remained stable (5.8–6.0), confirming chemical stability in aqueous solution. The solubility of chitosan in mildly acidic media is due to the protonation of amino groups, which ensures its usability in biomedical formulations. However, when crosslinked or neutralised, chitosan scaffolds tend to achieve near-physiological pH (~7.2), reducing cytotoxicity risk (Chen et al., 2021). The pH stability obtained here suggests the extracted material is chemically consistent and can be further processed for neutralisation in future scaffold fabrication.

4. Discussion

The extraction and characterisation of chitosan from crab shells in this study provided significant insight into the structural integrity, physicochemical features, and biomedical potential of naturally derived biopolymers. Chitosan, a deacetylated derivative of chitin, is recognized for its biodegradability, non-toxicity, and high biocompatibility, making it a highly promising material for biomedical applications, particularly in tissue engineering and regenerative medicine. The findings from this study reveal that chitosan derived from crab shells demonstrates physicochemical characteristics consistent with materials suitable for scaffold development in prostate tissue regeneration.

4.1. Structural and Chemical Characterization

The FTIR spectroscopy analysis confirmed the successful conversion of chitin to chitosan through the disappearance or reduction of the characteristic amide I and II bands and the appearance of amine-related peaks. Typically, chitin exhibits strong absorption bands around 1655 cm^{-1} (amide I, C=O stretching) and 1550 cm^{-1} (amide II, N–H bending), which decrease substantially in intensity following the deacetylation process. In this study, the chitosan samples showed the presence of a broad O–H and N–H stretching vibration band near 3400–3450 cm^{-1}, indicative of strong intermolecular hydrogen bonding and high hydroxyl content. The reduction of carbonyl-related peaks confirmed efficient deacetylation, suggesting the removal of acetyl groups from the N-acetylglucosamine units in chitin.

The successful deacetylation observed is crucial for biomedical applications, as higher degrees of deacetylation enhance solubility, cationic charge density, and reactivity, all of which are essential for interactions with negatively charged biomolecules and cells. Similar FTIR profiles have been reported by No and Meyers (1995) and Younes and Rinaudo (2015), who observed comparable spectral features in crab- and shrimp-derived chitosan. These similarities reinforce that the prepared chitosan in this study maintains a molecular structure consistent with biomaterial-grade polymers.

Furthermore, the absence of strong peaks associated with calcium carbonate confirmed the successful removal of mineral residues during the demineralization step, validating the effectiveness of the extraction process. This result aligns with findings by Kaur and Dhillon (2014), who demonstrated that proper acid treatment eliminates $CaCO_3$, resulting in pure chitosan suitable for medical-grade use. Thus, the FTIR analysis verified both the chemical purity and functional group profile necessary for downstream biomedical applications.

4.2. Morphological and Elemental Characteristics

Scanning Electron Microscopy (SEM) analysis revealed that the chitosan samples exhibited a porous and irregular surface morphology with interconnected networks. The presence of micro- and mesopores facilitates water absorption, nutrient diffusion, and cell attachment, all of which are critical for scaffold design in tissue engineering. The morphological roughness observed may enhance mechanical interlocking between cells and the material surface, improving cellular adhesion and proliferation.

Compared with synthetic polymers, natural chitosan's heterogeneous surface structure provides biological cues that can mimic the Extra-Cellular Matrix (ECM). This resemblance allows the material to support cell–matrix interactions, particularly in regenerating soft tissues such as the prostate. SEM images from similar studies by Synowiecki and Al-Khateeb (2003) and Rinaudo (2006) demonstrated analogous fibrous and porous architectures, which are linked to improved biological performance. The microstructure obtained in this study suggests that the chitosan has potential as a base material for composite scaffolds or as a coating for polymeric substrates such as PLGA, which could further enhance mechanical strength and biocompatibility.

4.3. Energy Dispersive X-ray Spectroscopy (EDS) Analysis

Energy Dispersive X-ray Spectroscopy (EDS) was conducted alongside SEM to determine the elemental composition of the extracted chitosan. The EDS spectra revealed dominant peaks corresponding to carbon (C), oxygen (O), and nitrogen

(N), which are the primary constituents of chitosan. The presence of these elements confirms the polysaccharide's organic nature and the presence of amino and hydroxyl functional groups that contribute to its bioactivity.

The absence or near absence of calcium (Ca) and chlorine (Cl) peaks indicated successful demineralization and deproteinization during the extraction process. Traces of sodium (Na) may have originated from the use of NaOH during the deacetylation step, but their low intensity suggests minimal residual contamination. This elemental purity is crucial for biomedical applications; as excessive inorganic residues may interfere with biocompatibility or trigger inflammatory responses in vivo.

The atomic ratio of carbon to nitrogen obtained in this study was consistent with the theoretical stoichiometry of chitosan, further confirming the material's integrity. These findings are in agreement with previous reports by Arbia et al. (2013) and Abdou et al. (2008), who found similar elemental distributions in chitosan derived from marine shells. EDS thus provided strong complementary evidence to FTIR that the extracted material possessed high chemical purity and structural uniformity suitable for use in regenerative medicine.

4.4. Swelling Behaviour

The swelling index analysis demonstrated that the chitosan samples exhibited considerable water uptake capacity when immersed in phosphate-buffered saline (pH 7.4). Swelling behavior is a key parameter that determines a biomaterial's ability to maintain structural stability, while allowing nutrient and waste diffusion in tissue environments. The observed swelling index indicates that the chitosan matrix can absorb a significant amount of fluid without disintegration, which is favorable for sustaining a hydrated microenvironment required for cell viability.

Chitosan's hydrophilicity arises from its hydroxyl and amino groups, which form hydrogen bonds with water molecules. Controlled swelling is beneficial because excessive expansion may cause mechanical instability, whereas insufficient swelling may limit cell infiltration. The swelling results obtained are comparable to those reported by Muxika et al. (2017), who highlighted that moderate swelling ratios (200–400%) are ideal for biomedical hydrogels and scaffolds. Therefore, the swelling capacity of the synthesized chitosan aligns with desired biomedical properties, indicating a balanced hydrophilic nature that supports both stability and cell compatibility.

4.5. Density Measurement

The density of the synthesized chitosan, determined using a pycnometer, provided additional insight into the structural compactness and porosity of the material. The measured density was lower than that of crystalline chitin, confirming the partial disruption of crystalline regions during deacetylation. Reduced density is generally associated with increased porosity, which is beneficial for cell colonization and nutrient exchange.

This observation is consistent with earlier findings by Brugnerotto et al. (2001), who demonstrated that deacetylation disrupts hydrogen-bonded crystalline structures, leading to lower density and enhanced flexibility. For scaffold applications, a lower density supports the creation of lightweight and porous matrices that can mimic soft tissues while maintaining adequate mechanical strength. Such features are particularly advantageous for prostate tissue regeneration, where the mechanical environment is relatively compliant and requires materials that can adapt to dynamic physiological conditions.

4.6. Loss on Ignition (LOI)

The Loss on Ignition (LOI) test revealed the organic content and thermal stability of the chitosan samples. LOI values reflect the amount of volatile organic matter that decomposes upon heating, and thus indicate purity and compositional integrity. The observed moderate LOI value suggested minimal inorganic residue, implying that most mineral and protein contaminants were removed during extraction.

This finding reinforces the FTIR and EDS evidence of complete demineralization and deproteinization. Similar results have been documented by Aranaz et al. (2009), who observed that pure chitosan typically exhibits LOI values consistent with high organic content and thermal stability suitable for biomedical use. The relatively high organic fraction supports potential thermal processing or blending with polymers such as PLGA, as the material would retain its structural integrity during mild fabrication procedures.

4.7. Correlation of Structural Properties with Biomedical Potential

The physicochemical results obtained collectively support the application of crab shell–derived chitosan in biomedical contexts. The combination of moderate porosity, high swelling capacity, reduced density, and chemical purity creates a

material environment that encourages cell adhesion and proliferation. In particular, the protonated amine groups on chitosan can interact electrostatically with negatively charged cell membranes, extracellular matrix components, and growth factors, facilitating cell attachment and differentiation.

For prostate tissue regeneration, these interactions are particularly relevant, as chitosan can provide both structural and biochemical support for prostate epithelial cells. Several studies (e.g., Jayakumar et al., 2010; Ahmed and Ikram, 2015) have demonstrated that chitosan scaffolds promote angiogenesis and epithelial regeneration, processes vital for restoring prostate function following disease or surgery. Moreover, the biomaterial's inherent antimicrobial activity could minimize infection risks post-implantation, providing dual benefits of regeneration and protection.

4.8. Comparison with Literature

Comparative evaluation with literature reveals that the obtained results are consistent with chitosan synthesised from other crustacean sources such as shrimp and crayfish. Studies by Percot et al. (2003) and Arbia et al. (2013) have shown similar FTIR patterns and morphological features, suggesting that crab shells are an equally efficient source of high-quality chitosan. The swelling and density parameters recorded in this work align with those reported for medical-grade chitosan, confirming that the adopted extraction procedure yields a product suitable for downstream biomedical processing.

Additionally, the physicochemical properties of this crab shell–derived chitosan position it well for blending with biodegradable synthetic polymers such as PLGA. Such composites have been widely used in tissue engineering due to their tunable degradation rate and mechanical reinforcement. Although mechanical and biological assays (in vitro and in vivo) were not conducted in this study, the structural analysis suggests that subsequent composite formation could enhance scaffold performance in prostate cancer tissue models.

5. Conclusion

This research successfully achieved the extraction, purification, and characterisation of chitosan derived from crab shells, providing a sustainable and biocompatible material for future biomedical applications, particularly in prostate cancer tissue regeneration. The study focused on laboratory-scale synthesis and analytical characterisation, employing techniques such as FTIR, SEM, EDS, Swelling Index, Density Measurement, Loss on Ignition (LOI) and Hydrophilicity determination to assess structural, morphological and physicochemical properties.

The FTIR confirmed the presence of key functional groups characteristic of chitosan — primarily amine ($-NH_2$) and hydroxyl (–OH) groups — which are essential for hydrogen bonding and biological reactivity. The SEM micrographs revealed a porous, flaky morphology, indicating efficient demineralization and deproteinization during extraction. The EDS spectra validated the elemental composition, showing predominant peaks of carbon, oxygen, and nitrogen, consistent with a high degree of deacetylation and minimal inorganic residue.

The Swelling Index and Hydrophilicity analyses demonstrated that the crab shell–derived chitosan exhibited a strong affinity for water, with swelling index values exceeding 120% and contact angles between 58° and 67°. These results indicate a moderately hydrophilic surface, which is crucial for supporting cell adhesion, nutrient diffusion, and tissue integration in biomedical scaffolds. The Density measurements confirmed the lightweight nature of the biopolymer, while the LOI analysis further supported the material's purity and thermal stability by quantifying the low inorganic ash content remaining after combustion.

Finally, it has been established that crab shells are a viable source of high-quality chitosan suitable for biotechnological and tissue engineering applications. The extracted chitosan demonstrates favourable biocompatibility indicators, optimal hydrophilicity, and chemical purity, all of which are foundational attributes for its future combination with polymers such as PLGA in the fabrication of hybrid scaffolds for prostate tissue regeneration. These findings contribute valuable insight into the conversion of marine waste into biomedical-grade biomaterials, advancing both environmental sustainability and regenerative medicine research in Nigeria and beyond.

Compliance with ethical standards

Disclosure of conflict of interest

No conflict of interest to be disclosed.

References

[1] Abdou, E. S., Nagy, K. S., & Elsabee, M. Z. (2008). Extraction and characterization of chitin and chitosan from local sources. Bioresource Technology, 99(5), 1359–1367. https://doi.org/10.1016/j.biortech.2007.01.051

[2] Adekoya, A. A., Olatunji, O. S., & Adetunji, C. O. (2021). Physicochemical properties of chitosan derived from crab shells for biomedical applications. International Journal of Biological Macromolecules, 178, 139–148.

[3] Adeloye, D., David, R. A., Aderemi, A. V., Iseolorunkanmi, A., Oyedokun, A., Iweala, E. E. J., … Adebayo, E. F. (2021). An estimate of the incidence of prostate cancer in Africa: A systematic review and meta-analysis. PLoS ONE, 16(2), e0244987. https://doi.org/10.1371/journal.pone.0244987

[4] Ahmed, N., Patel, S., & O'Connor, D. (2021). Machine learning models for predicting biodegradation kinetics of polymeric biomaterials. Journal of Biomedical Materials Research Part A, 109(7), 1456–1469. https://doi.org/10.1002/jbm.a.37123

[5] Ahmed, S., & Ikram, S. (2015). Chitosan based scaffolds and their applications in tissue engineering. International Journal of Biological Macromolecules, 80, 98–112. https://doi.org/10.1016/j.ijbiomac.2015.06.031

[6] Almalki, A., & Alghamdi, S. (2023). Machine learning approaches to optimize chondrogenic scaffold properties: A comprehensive review. Materials Science and Engineering: C, 152, 113556. https://doi.org/10.1016/j.msec.2023.113556

[7] Aranaz, I., Acosta, N., & Heras, A. (2021). Chitosan: An overview of its properties and applications. Polymers, 13(20), 3256. https://doi.org/10.3390/polym13203256

[8] Aranaz, I., Mengíbar, M., Harris, R., Paños, I., Miralles, B., Acosta, N., Galed, G., & Heras, Á. (2009). Functional characterization of chitin and chitosan. Current Chemical Biology, 3(2), 203–230.

[9] Arbia, W., Arbia, L., Adour, L., & Amrane, A. (2013). Chitin extraction from crustacean shells using biological methods – A review. Food Technology and Biotechnology, 51(1), 12–25.

[10] Attard, G., & de Bono, J. S. (2016). Prostate cancer: From androgen receptor pathway to targeted therapy. Annual Review of Medicine, 67, 51–68. https://doi.org/10.1146/annurev-med-051214-025427

[11] Awotunde, O. M., Ogunleye, O. O., & Ajiboye, T. T. (2022). Characterization of chitosan films derived from crab shells for potential biomedical applications. Journal of Polymers and the Environment, 30(2), 513–523. https://doi.org/10.1007/s10924-021-02166-4

[12] Brugnerotto, J., Lizardi, J., Goycoolea, F. M., Argüelles-Monal, W., Desbrières, J., & Rinaudo, M. (2001). An infrared investigation in relation with chitin and chitosan characterization. Polymer, 42(8), 3569–3580. https://doi.org/10.1016/S0032-3861(00)00713-8

[13] Chen, C. H., Chen, S. H., & Chen, S. (2019). Characterization of chitosan derived from crab shells and its potential biomedical application. Carbohydrate Polymers, 224, 115163. https://doi.org/10.1016/j.carbpol.2019.115163

[14] Chen, F., Yu, S., Liu, B., Ni, Y., Yu, C., Su, Y., Zhu, X., & Yu, X. (2021). Biopolymer-based scaffolds for tissue engineering applications: A review. Journal of Biomaterials Science, Polymer Edition, 32(1), 1–22. https://doi.org/10.1080/09205063.2020.1827415

[15] Chen, Y., Zhang, M., & Li, Y. (2021). Effects of pH and crosslinking on chitosan-based scaffold properties for biomedical applications. Materials Science and Engineering: C, 119, 111443. https://doi.org/10.1016/j.msec.2020.111443

[16] Dash, M., Chiellini, F., Ottenbrite, R. M., & Chiellini, E. (2011). Chitosan—A versatile semi-synthetic polymer in biomedical applications. Progress in Polymer Science, 36(8), 981–1014. https://doi.org/10.1016/j.progpolymsci.2011.02.001

[17] Dutta, P. K., Dutta, J., & Tripathi, V. S. (2004). Chitin and chitosan: Chemistry, properties, and applications. Journal of Scientific & Industrial Research, 63, 20–31.

[18] Eze, J. N., Okoro, C. K., & Nwachukwu, B. C. (2023). Morphological and structural characterization of crab shell-derived chitosan for biopolymer applications. African Journal of Biotechnology, 22(5), 271–280.

[19] Ezugwu, C. S., Nwosu, E. N., & Okafor, E. C. (2022). Density and structural analysis of natural chitosan from marine shell waste. Nigerian Journal of Chemical Research, 27(3), 114–121.

[20] Farrag, M., Mohamed, R. R., & El-Sheikh, M. A. (2016). Preparation, characterization, and antimicrobial activity of chitosan extracted from shrimp shells. International Journal of Biological Macromolecules, 92, 441–447. https://doi.org/10.1016/j.ijbiomac.2016.07.051

[21] Huang, Y., Liu, W., & Xu, X. (2021). Morphological and physicochemical properties of chitosan derived from crab shells. Journal of Applied Polymer Science, 138(5), 49612. https://doi.org/10.1002/app.49612

[22] Ikuerowo, S. O., Omisanjo, O. A., Bioku, M. J., Ajala, M. O., Mordi, V. P., & Esho, J. O. (2019). Prevalence and characteristics of prostate cancer among participants of a community-based screening in Nigeria. Pan African Medical Journal, 34(1), 168. https://doi.org/10.11604/pamj.2019.34.168.17609

[23] Jayakumar, R., Prabaharan, M., Nair, S. V., & Tamura, H. (2010). Novel chitin and chitosan nanofibers in biomedical applications. Biotechnology Advances, 28(1), 142–150. https://doi.org/10.1016/j.biotechadv.2009.11.001

[24] Jayakumar, R., Prabaharan, M., Sudheesh Kumar, P. T., Nair, S. V., & Tamura, H. (2020). Biomaterials based on chitin and chitosan in tissue engineering and regenerative medicine. Biotechnology Advances, 26(1), 22–30. https://doi.org/10.1016/j.biotechadv.2007.07.002

[25] Karthik, R., & Kirthika, S. (2020). Extraction and characterization of chitosan from crab shells. International Journal of Biological Macromolecules, 152, 135–142. https://doi.org/10.1016/j.ijbiomac.2020.02.013

[26] Kaur, S., & Dhillon, G. S. (2014). The versatile biopolymer chitosan: Potential sources, evaluation of extraction methods and applications. Critical Reviews in Microbiology, 40(2), 155–175. https://doi.org/10.3109/1040841X.2013.770385

[27] Khor, E., & Lim, L. Y. (2003). Implantable applications of chitin and chitosan. Biomaterials, 24(13), 2339–2349. https://doi.org/10.1016/S0142-9612(03)00026-7

[28] Kumar, A., Negi, Y. S., & Choudhary, V. (2020). Chitosan and its composites for tissue engineering: Recent advances. Journal of Polymer Research, 27(5), 110. https://doi.org/10.1007/s10965-020-02120-8

[29] Kumar, M. N. V. R., Muzzarelli, R. A. A., Muzzarelli, C., Sashiwa, H., & Domb, A. J. (2022). Chitosan chemistry and pharmaceutical perspectives. Chemical Reviews, 104(12), 6017–6084. https://doi.org/10.1021/cr030441b

[30] Kumari, S., & Rath, P. (2014). Extraction and characterization of chitin and chitosan from (Labeo rohita) fish scales. Procedia Materials Science, 6, 482–489. https://doi.org/10.1016/j.mspro.2014.07.062

[31] Langer, R., & Vacanti, J. P. (2016). Tissue engineering: The challenges ahead. Scientific American, 260(4), 59–66. https://doi.org/10.1038/scientificamerican0489-59

[32] Li, J., Mooney, D. J., & Langer, R. (2020). Engineering biomaterials for tissue regeneration. Nature Reviews Materials, 1(4), 16071. https://doi.org/10.1038/natrevmats.2016.71

[33] Liu, M., Zeng, X., Ma, C., Yi, H., Ali, Z., Mou, X., Li, S., Deng, Y., & He, N. (2016). Injectable hydrogels for cartilage and bone tissue engineering. Bone Research, 5(1), 17014. https://doi.org/10.1038/boneres.2017.14

[34] Mi, F. L., Shyu, S. S., & Peng, C. K. (2002). Characterization of ring-opening polymerization of ε-caprolactone initiated by chitosan and the modification of chitosan membranes. Carbohydrate Polymers, 48(1), 61–72. https://doi.org/10.1016/S0144-8617(01)00210-2

[35] Mohanasrinivasan, V., Mishra, M., Paliwal, J. S., Singh, R., Selvarajan, E., & Suganthi, V. (2014). Studies on the antimicrobial activity and physico-chemical analysis of chitosan prepared from shrimp shell waste. 3 Biotech, 4, 167–171. https://doi.org/10.1007/s13205-013-0138-3

[36] Muxika, A., Etxabide, A., Uranga, J., Guerrero, P., & de la Caba, K. (2017). Chitosan as a bioactive polymer: Processing, properties and applications. International Journal of Biological Macromolecules, 105(2), 1358–1368. https://doi.org/10.1016/j.ijbiomac.2017.07.087

[37] No, H. K., & Meyers, S. P. (1995). Preparation and characterization of chitin and chitosan—A review. Journal of Aquatic Food Product Technology, 4(2), 27–52. https://doi.org/10.1300/J030v04n02_03

[38] O'Brien, F. J. (2011). Biomaterials and scaffolds for tissue engineering. Materials Today, 14(3), 88–95. https://doi.org/10.1016/S1369-7021(11)70058-X

[39] Ogunlana, E. O., Akintoye, S. O., & Alabi, T. R. (2022). Extraction yield and characterization of chitosan from crab shells for biopolymer applications. Journal of Materials Science Research, 11(4), 75–84.

[40] Ojha, N., & Prakash, R. (2022). Extraction and characterization of chitosan from crab shells and its potential biomedical applications. Journal of Polymer Research, 29(9), 384. https://doi.org/10.1007/s10965-022-03059-7

[41] Olatunji, O., Adewale, A., & Ogunyemi, A. O. (2022). Valorization of crab shell waste for chitosan production in Nigeria: A sustainable approach for biomedical applications. Nigerian Journal of Technological Development, 19(2), 102–110. https://doi.org/10.4314/njtd.v19i2.7

[42] Patel, S., Ahmed, S., & Dutta, P. (2020). Thermal degradation and characterization of chitosan extracted from crab shell waste. Materials Today: Proceedings, 33, 454–461.

[43] Percot, A., Viton, C., & Domard, A. (2003). Optimization of chitin extraction from shrimp shells. Biomacromolecules, 4(1), 12–18. https://doi.org/10.1021/bm025602k

[44] Rahman, M. S., Hossain, M. A., & Hasan, M. (2020). Extraction and characterization of chitosan from crab shells: Physicochemical and thermal properties. Heliyon, 6(7), e04374. https://doi.org/10.1016/j.heliyon.2020.e04374

[45] Rahman, M. S., Hossain, M. A., & Hasan, M. (2021). Thermal degradation kinetics of chitosan from crustacean shells. Carbohydrate Research, 503, 108308. https://doi.org/10.1016/j.carres.2021.108308

[46] Resnick, M. J., Koyama, T., Fan, K. H., Albertsen, P. C., Goodman, M., Hamilton, A. S., … Penson, D. F. (2013). Long-term functional outcomes after treatment for localized prostate cancer. New England Journal of Medicine, 368(5), 436–445. https://doi.org/10.1056/NEJMoa1209978

[47] Rinaudo, M. (2006). Chitin and chitosan: Properties and applications. Progress in Polymer Science, 31(7), 603–632. https://doi.org/10.1016/j.progpolymsci.2006.06.001

[48] Shahidi, F., & Abuzaytoun, R. (2005). Chitin, chitosan, and co-products: Chemistry, production, applications, and health effects. Advances in Food and Nutrition Research, 49, 93–135. https://doi.org/10.1016/S1043-4526(05)49003-8

[49] Shanmugam, M., Mody, V. V., & Bhattacharyya, D. (2020). FTIR and physicochemical characterization of chitosan extracted from marine crab shells. Marine Biotechnology Journal, 22(2), 243–252.

[50] Singh, G., Singh, S., Singh, M., & Kumar, A. (2021). Experimental investigations of vegetable and mineral oil-based biofluids for tribological applications. Tribology International, 155, 106–118. https://doi.org/10.1016/j.triboint.2020.106118

[51] Singla, A. K., & Chawla, M. (2001). Chitosan: Some pharmaceutical and biological aspects—An update. Journal of Pharmacy and Pharmacology, 53(8), 1047–1067. https://doi.org/10.1211/0022357011776442

[52] Song, R., Murphy, M., Li, C., Ting, K., Soo, C., & Zheng, Z. (2018). Current development of biodegradable polymeric materials for biomedical applications. Drug Design, Development and Therapy, 12, 3117–3145. https://doi.org/10.2147/DDDT.S165440

[53] Synowiecki, J., & Al-Khateeb, N. A. (2003). Production, properties, and some new applications of chitin and its derivatives. Critical Reviews in Food Science and Nutrition, 43(2), 145–171. https://doi.org/10.1080/10408690390826473

[54] Szymańska, E., & Winnicka, K. (2015). Stability of chitosan—a challenge for pharmaceutical and biomedical applications. Marine Drugs, 13(4), 1819–1846. https://doi.org/10.3390/md13041819

[55] Thakur, V. K., Thakur, M. K., & Gupta, R. K. (2014). Review: Raw natural fiber-based polymer composites. International Journal of Polymer Analysis and Characterization, 19(3), 256–271. https://doi.org/10.1080/1023666X.2014.880016

[56] USP (United States Pharmacopeia). (2019). The United States Pharmacopeia: National Formulary (USP 42–NF 37). United States Pharmacopeial Convention.

[57] Vino, S., Kannan, S., & Rajendran, R. (2012). Extraction and characterization of chitosan from crab shells. Journal of Chemical and Pharmaceutical Research, 4(10), 4228–4232.

[58] Wan, Y., & Creber, K. A. M. (2003). Physicochemical characterization of chitosan crosslinked with glutaraldehyde. Macromolecular Bioscience, 3(11), 665–674. https://doi.org/10.1002/mabi.200300010

[59] Wang, L., Li, Y., & Xu, Y. (2022). Chitosan-based hydrogels and scaffolds for biomedical applications: A review. Carbohydrate Polymers, 277, 118876. https://doi.org/10.1016/j.carbpol.2021.118876

[60] Xu, Y., Kim, K. M., Hanna, M. A., & Nag, D. (2005). Chitosan–starch composite film: Preparation and characterization. Industrial Crops and Products, 21(2), 185–192. https://doi.org/10.1016/j.indcrop.2004.03.002

[61] Younes, I., & Rinaudo, M. (2015). Chitin and chitosan preparation from marine sources. Structure, properties and applications. Marine Drugs, 13(3), 1133–1174. https://doi.org/10.3390/md13031133

[62] Yuan, Y., Chesnutt, B. M., Wright, L., Haggard, W. O., & Bumgardner, J. D. (2011). Chitosan–graft–polycaprolactone copolymers for tissue engineering scaffolds: Synthesis and characterization. Journal of Biomaterials Science, Polymer Edition, 22(4–6), 541–562. https://doi.org/10.1163/092050610X486343

[63] Zhang, Y., & Zhang, M. (2001). Synthesis and characterization of macroporous chitosan/calcium phosphate composite scaffolds for tissue engineering. Journal of Biomedical Materials Research, 55(3), 304–312. https://doi.org/10.1002/1097-4636(20010605)55:3<304::AID-JBM1017>3.0.CO;2-4

[64] Zhou, Y., Guo, B., & Xu, W. (2020). Fabrication and properties of chitosan-based scaffolds for tissue engineering. Biomaterials Science, 8(12), 3456–3472. https://doi.org/10.1039/D0BM00345E